Dielectric broadband meta-vector-polarizers based on nematic liquid crystal

Gui-Geng Liu,[1,2] Yun-Han Lee,[2] Yuge Huang,[2] Zheyuan Zhu,[2] Guanjun Tan,[2] Meng-Qiang Cai,[1] Ping-Ping Li,[1] Dan Wang,[1] Yongnan Li,[1] Shuo Pang,[2] Chenghou Tu,[1,a] Shin-Tson Wu,[2,b] and Hui-Tian Wang[1,3,c]

[1]*MOE Key Laboratory of Weak Light Nonlinear Photonics and School of Physics, Nankai University, Tianjin 300071, China*
[2]*College of Optics and Photonics, University of Central Florida, Orlando, Florida 32816, USA*
[3]*National Laboratory of Solid State Microstructures and School of Physics, Nanjing University, Nanjing 210093, China and Collaborative Innovation Center of Advanced Microstructures, Nanjing University, Nanjing 210093, China*

Polarizer, as an indispensable optical element, has been widely used in various optical systems, which splits a beam into two beams of orthogonal linear polarizations. Due to the appearance of the vector optical field (VOF) and its unique properties, the vector polarizer also meets the requirement in a wide variety of applications. Here we present and demonstrate the realization of dielectric broadband vector polarizer, being in fact a liquid-crystal-based space-variant uniaxial crystal (LC-SV-UAC), which is made by a wedged thin cell adhered with space-variant photo-aligned dichroic dye films and filled with the nematic liquid crystal with a thickness of tens of microns. The vector polarizer works based on the birefringent mechanism to spatially separate the orthogonally polarized ordinary and extraordinary beams. The vector polarizers via a LC-SV-UAC have the advantages of mass-production and easy fabrication of large-size and complex structures. In particular, the high-performance broadband vector polarizers we presented and fabricated can not only flexibly tailor the polarization structures and the intensity patterns of optical fields but also act as a high-efficiency generator of VOF, and a key element for realizing the VOF laser and for fabricating the novel photon states in the future. © *2017 Author(s). All article content, except where otherwise noted, is licensed under a Creative Commons Attribution (CC BY) license (http://creativecommons.org/licenses/by/4.0/).* https://doi.org/10.1063/1.5006016

I. INTRODUCTION

As is well known, polarizers, which split a beam into two beams of orthogonal linear polarizations,[1] are a kind of greatly important optical elements because they are indispensable in various optical systems. The traditional polarizers can work mainly via four different mechanisms, including the interference effect, the Brewster's effect, the polarization selective absorption, and the birefringent effect. The traditional polarizers via the birefringent effect have some advantages such as high damage threshold, broadband, and perfect polarization purity, but are space-invariant.

Structured optical fields,[2,3] with space-variant intensity, phase, and polarization, have found useful applications in optical trapping,[4–6] micro-processing,[7,8] quantum information,[9,10] high-resolution microscopy,[11,12] remote sensing and optical communication (e.g., in fiber and in free space),[13–17] and so on. Among them, the structured optical fields with space-variant polarization are in fact vector optical fields (VOFs).[2,18,19] To spatially tailor the polarization and then to create the VOFs, some devices have been adopted, including the spatial light modulators (SLMs),[18–21] the space-variant

---

[a]Electronic mail: tuchenghou@nankai.edu.cn
[b]Electronic mail: swu@ucf.edu
[c]Electronic mail: htwang@nju.edu.cn

wave plate,[22,23] the subwavelength grating,[24] and the metasurface.[25–27] To widely use the VOFs in practical applications due to the unique properties,[2,4–6,28–30] like the traditional polarizers, vector polarizers are also indispensable in various optical systems. Therefore, it is of great importance to explore the vector polarizers for tailoring the optical fields and for satisfying the requirements in various applications.

Although subwavelength metal structures or metasurfaces[27,31] have been used to produce the vector polarizers, they are not only costly but also difficult to fabricate the high-quality and large-size complex structures. Therefore, one good choice for realizing the vector polarizer is to use the space-variant uniaxial crystal (SV-UAC) based on the birefringent mechanism. Here our motivation is to provide a solution of high-performance and large-size vector polarizers with arbitrary spatial structures. We present a universal method to design and to then fabricate various vector polarizers based on the liquid-crystal-based SV-UAC (LC-SV-UAC), to meet the demands in various optical systems. The key to achieve our aim is able to control the patterned alignments of liquid crystal (LC) molecules, which are determined by the patterned orientations of the dichroic dye molecules. The patterned orientations of the LC molecules can be realized by a non-contact photo-alignment technique,[32,33] when the polarization-sensitive dichroic dye is irradiated by the vector optical field (VOF) with the predesigned space-variant polarization. We fabricate successfully the vector polarizers, which are a kind of wedged LC-SV-UACs, to flexibly modulate the spatial structures of polarization and intensity of the optical fields. Since the vector polarizers we presented work based on the birefringent mechanism, they have the advantages of broadband, large-size, and perfect polarization purity.

II. PRINCIPLE AND FABRICATION OF VECTOR POLARIZERS

A. Principle

As an example, Fig. 1 depicts the configuration of a vector polarizer, which is composed of two glass substrates adhered with photo-aligned dichroic dye films and the LC molecules filled between them. In particular, the two photo-aligned dichroic brilliant-yellow dye (hereafter briefly as "dye")
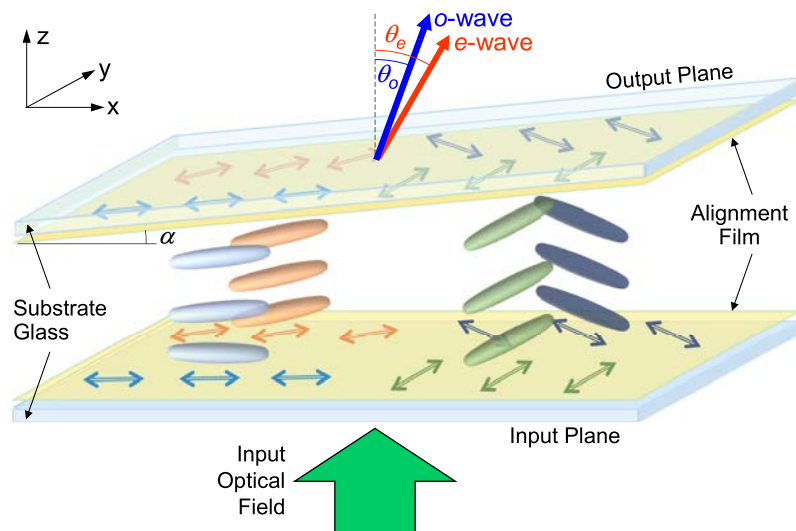

FIG. 1. Configuration of a vector polarizer (a wedged LC-SV-UAC device). The polarization-sensitive brilliant yellow dye was spin-coated onto the square glass substrates as the alignment films. The plastic spherical spacers with different diameters of 1.0 and 40.0 μm were dispensed at two opposite edges of the square substrates to create a wedged cell with a wedge angle $\alpha \approx 0.15°$. After exposure with a predesigned VOF at a wavelength $\lambda = 488$ nm, the cell was filled with the LC mixture (LCM-2018, $\Delta n = 0.42$) by capillary action. The orientation of the LC molecule is parallel to the alignment direction of the dye, which is perpendicular to the polarization of the exposed light. The o-wave with a deflection angle of θ_o is linearly polarized and perpendicular to the alignment direction. The e-wave with a deflection angle of θ_e is linearly polarized and parallel to the alignment direction.

films have the space-variant molecule orientations to arrange the highly birefringent nematic LC molecules sandwiched between them, to finally form a wedged LC-SV-UAC. A single LC molecule can be considered as an ellipsoid and a local small "uniaxial crystal," whose orientation is parallel to the local alignment direction of the dye films, and the local optic axis is parallel to the local LC orientation. Like in a homogenous uniaxial crystal, in a LC-SV-UAC, there have two orthogonally polarized ordinary wave (*o*-wave) and extraordinary wave (*e*-wave). For LC-SV-UAC, however, the *o*- and *e*-wave fields are the VOFs with the space-variant polarization states instead of space-invariant ones. The wedged structure in LC-SV-UAC is adopted to spatially separate the two orthogonally *o*- and *e*-wave fields, based on both the prism and birefringent effects.

As shown in Fig. 1, when light is normally incident on the input plane of the wedged LC-SV-UAC, after it transmits through the high birefringent LC layer, the *o*- and *e*-waves will be refracted at two different angles deviating from the incident direction.[34] When light propagates perpendicular to the optic axis, the refractive indices for the *o*- and *e*-waves are approximately n_o and n_e, respectively. When the input optical field propagates along the *z* axis, according to the Snell law, the *o*- and *e*-waves propagating in the *x*-*z* plane have the deflection angles of θ_o and θ_e, respectively, which are as follows:

$$\theta_o \approx \sin^{-1}(n_o \sin \alpha / n_{air}) - \alpha \approx \sin^{-1}(n_o \sin \alpha) - \alpha, \tag{1}$$

$$\theta_e \approx \sin^{-1}(n_e \sin \alpha / n_{air}) - \alpha \approx \sin^{-1}(n_e \sin \alpha) - \alpha, \tag{2}$$

where $n_{air} \approx 1$ is the refractive index of the air. Thus, the separation angle between the *o*- and *e*-waves, $\theta_e - \theta_o$, is about 0.06° in our experiments. The polarization directions of the *o*- and *e*-waves are perpendicular and parallel to the optic axis of the local LC molecules, respectively. By patterning the alignment of the LC molecules through photo-alignment technology, a desired vector polarizer (wedged LC-SV-UAC) is easily fabricated as follows.

B. Fabrication

A vector polarizer or a wedged LC-SV-UAC, as shown in Fig. 1, is composed of two glass substrates adhered with photo-aligned dichroic dye films and the LC molecules filled between them. To fabricate a vector polarizer, there are three steps: (1) fabricating the empty wedged cell, (2) photo-aligning the dichroic brilliant-yellow dye films, and (3) filling the nematic LC molecules to the empty wedged cell.

1. Fabrication of empty wedged cells

The polarization-sensitive dichroic brilliant-yellow dye (Sigma-Aldrich, US) was adopted to form the photo-aligned films and then to orient the LC molecules.[32,33] Two square BK7 glass plates with the same dimensions of 15×15 mm^2 were used as the substrates. The dye was mixed with dimethylformamide (DMF) solvent at 0.5 wt. %. To improve the stability of dye, the reactive mesogen RM257 was added at 0.1 wt. %. After vortexing for 1 min, the solution was purified twice. Before spin-coating the solution, the two substrates were cleaned for 20 min in the UV-ozone machine. The dye-doped solution was spin-coated onto the two substrates at 800 rpm for 20 s and then 1500 rpm for 40 s. The coated substrates were baked at 95 °C for 30 min to remove the remaining solvent and to strengthen the adhesion of the azodye molecules on the substrates. The thickness of the dye film was measured to be ∼50 nm. The two substrates were then assembled together using the epoxy glue. Two kinds of plastic spherical spacers with different diameters (1.0 μm and 40.0 μm) were mixed with the epoxy glue, respectively, and subsequently were sandwiched between the two opposite edges of the two substrates adhered with the dye films, respectively. After sealed with the epoxy glue, the empty wedged cell with a wedge angle of $\alpha \sim 0.15°$ is finally fabricated.

2. Fabrication of photo-aligned dye films

The dye films adhered on the empty wedged cell were exposed by the predesigned optical field with a wavelength of $\lambda = 488$ nm (Ar$^+$ laser) and a power density of ∼10 mW/cm^2, for 90 min to align the dye molecules. Since the dye molecules orient along the local polarization directions, to achieve the desired space-variant alignment pattern for the dye films by the photo-alignment technique,[32,33] the optical field used for exposure must be a local linearly polarized VOF.
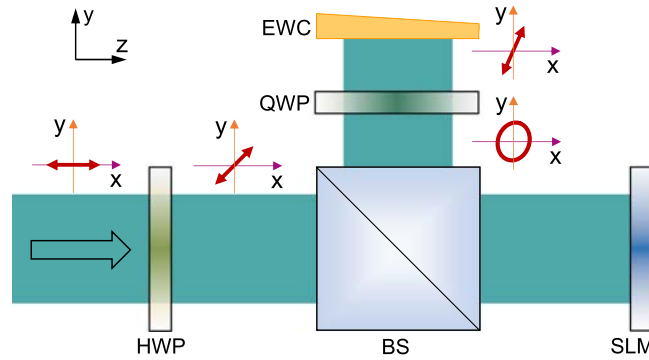
FIG. 2. Exposing optical setup for fabricating meta-vector-polarizer. EWC—empty wedged cell, HWP—half-wave plate, QWP—quarter-wave plate, BS—polarization-independent beam splitter, SLM—spatial light modulator.

Therefore, as a unique candidate, the optical field used for photo-alignment must be a VOF with the demanded spatial structure of linear polarization. The exposing optical system including the generation unit of the VOF and their details are given in Subsection II B 3. After exposure, the aligned dye films are fabricated.

3. Exposing optical system and generation of VOF

The optical setup for exposure is shown in Fig. 2, which is in fact a generation system of the VOF when excluding the empty wedged cell. The input x-polarized Ar$^+$ laser at $\lambda = 488$ nm was firstly expanded and collimated to a parallel beam. A half-wave plate (HWP) rotates the polarization by an angle of $45°$ with respect to the x axis. After passing through the polarization-independent beam splitter (BS), the laser beam was normally incident onto a phase-only SLM (1920×1152 pixels with a pixel size of 9.2×9.2 μm^2, Meadowlark Optics, Inc., US). The light incident onto the SLM can be written as $E_0(\hat{\mathbf{e}}_x + \hat{\mathbf{e}}_y)$, where $\hat{\mathbf{e}}_x$ and $\hat{\mathbf{e}}_y$ are the unit vectors in the x and y axes. The used SLM modulates only the y-polarized wave to acquire a phase retardation δ with respect to the x-polarized wave. The x- and y-polarized waves reflected by the SLM are reflected by BS again and then pass through a quarter-wave plate (QWP) with the optical axis orientated at $45°$, thus the generated optical field incident on the empty wedged cell can be written as $E_0 \exp(-i\delta/2)[\cos(\delta/2)\hat{\mathbf{e}}_x + \sin(\delta/2)\hat{\mathbf{e}}_y]$. Clearly, this is a linearly polarized field with a polarization angle $\delta/2$ and an additional phase $\delta/2$. It should be pointed out that δ can be space-variant and its spatial distribution is easily designed and controlled by a computer-generated hologram. Thus, the generated optical field incident on the empty wedged cell is a VOF with space-variant linear polarization distribution depending on the spatial geometry of δ, which is then used to expose the dye films. The orientation of the polarization-sensitive dye molecules is perpendicular to the local polarization direction of the exposuring VOF.

4. Fabrication of vector polarizer

The nematic LC molecules (LCM-2018 with $\Delta n = 0.42$) were infiltrated into the gap of the fabricated empty wedged cell adhered with the aligned dye films, by the capillary flow effect. After infiltration, a vector polarizer (i.e., a wedged LC-SV-UAC) was successfully fabricated. The high birefringence helps to spatially separate an incident optical field into two orthogonally o- and e-polarized waves. It should be pointed out that the LC molecules filled within the wedged LC-SV-UAC will be aligned along the orientations of the photo-aligned dye molecules in the dye films.

III. RESULTS

A. Separation of orthogonal polarization

To verify the fact that the polarizations of the o-wave and e-wave are indeed perpendicular and parallel to the alignment direction of the LC molecules, respectively, we firstly fabricated a vector polarizer consisting of four alignment directions at $-45°$, $45°$, $0°$, and $90°$ in the x-y plane, which occupy the first to the fourth quadrant, respectively [Fig. 3(a)]. In the optical setup to test the fabricated
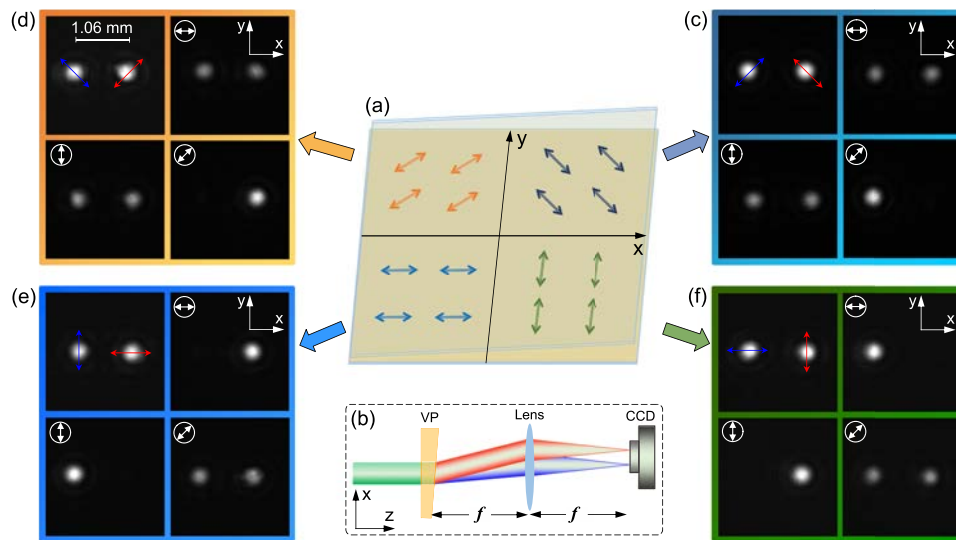
FIG. 3. Polarization characteristics of the *o*- and *e*-waves refracted from the vector polarizer. (a) The fabricated vector polarizer (VP), which was divided into four regions, where the LC molecules are aligned at −45°, 45°, 0°, and 90° from the first to the fourth quadrant in the *x*-*y* plane, respectively. (b) The optical setup to test the vector polarizer. The input laser is circularly polarized and passes through one quadrant for each time. (c)–(f) show the focal field patterns of the total intensity and the different polarized components of the beams refracted from the vector polarizer, when the first, second, third, and fourth quadrants of the vector polarizer are illuminated in turn, respectively. The left and right spots belong to the *o*- and *e*-waves, respectively. The blue and red dual-arrows represent the polarization directions of the *o*- and *e*-waves, and the white dual-arrows surrounded by a circle stand for the polarization orientation of the polarizer.

vector polarizer [Fig. 3(b)], a collimated input beam at λ = 442 nm illuminated normally the vector polarizer along the *z* axis, the *o*- and *e*-waves output from the vector polarizer were separated at the output plane. The circular polarization of the input light ensures that the *o*- and *e*-waves have both the space-invariant amplitude. For each test, the incident light illuminated only one of the four quadrants of the vector polarizer. The vector polarizer was placed at the front focal plane of a lens with a focal length *f* = 1 m. To confirm the properties of the *o*- and *e*-waves refracted from the four quadrants, a CCD was placed at the back focal plane of the lens, and a linear polarizer was inserted in front of the CCD and orientated in three different directions shown by the white dual-arrows surrounded by a circle in Figs. 3(c)–3(f). When the first, second, third, and fourth quadrants of the vector polarizer were illuminated in turn, the focal field patterns of the corresponding refracted beams are shown in Figs. 3(c)–3(f), respectively. The left and right spots in Figs. 3(c)–3(f) are conformed to be the focal points of the *o*- and *e*-waves, respectively. As shown in Fig. 2, the polarization directions of the *o*- and *e*-waves are indeed perpendicular and parallel to the alignment direction, respectively.

B. Spatial modulation of polarization

The polarization characteristics of the *o*- and *e*-waves refracted from the vector polarizer have been confirmed experimentally. Based on this fact, tailoring the optical fields in spatial domain can also be realized through spatially customizing the alignment direction of the vector polarizer. The first example is a radially aligned vector polarizer, whose alignment direction is shown in the inset of Fig. 4. As demonstrated above, to fabricate the radially aligned vector polarizer, the VOF used for the exposure must be the azimuthally polarized vector field. The radially aligned vector polarizer can separate an incident circularly polarized optical field into a pair of orthogonally, radially, and azimuthally polarized vector fields, whose polarization distributions are shown in Figs. 4(b) and 4(c). Of course, we easily presume that the wave refracted from the radially aligned vector polarizer has the azimuthally (radially) polarized vector field only, under the incidence of radially (azimuthally) polarized vector optical field. Under the incidence of the horizontally linearly polarized wave, the *o*- and *e*-waves refracted from the radially aligned vector polarizer will also be azimuthally and radially polarized, but with nonuniform intensity, as shown in Figs. 4(d) and 4(e).
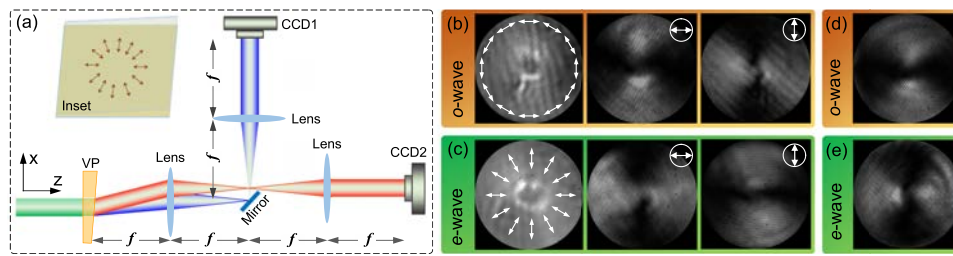
FIG. 4. Radially aligned meta-vector-polarizer. (a) Experimental setup to test the radially aligned meta-vector-polarizer, as shown in the inset. [(b) and (c)] The intensity patterns of the *o*- and *e*-waves refracted from the radially aligned vector polarizer, respectively, under the incidence of circularly polarized light. [(d) and (e)] The intensity patterns of the *o*- and *e*-waves refracted from the radially aligned vector polarizer, respectively, under the incidence of horizontally linearly polarized light. (b)–(e) have the same dimensions of 5×5 mm^2.

In fact, the alignment pattern of the vector polarizer should be able to be arbitrarily customized. We design and fabricate a more complex vector polarizer. The second example is a vector polarizer composed of four Archimedes spirals, which has a continuously changed alignment pattern of the LC molecules. The orientation angle φ of the LC molecule (or the optic axis) obeys $\varphi = 2\pi r/r_0 + 2\phi$ within $0 \le (2\pi r/r_0 + 2\phi) < \pi$ but $\varphi = 2\pi - (2\pi r/r_0 + 2\phi)$ within $\pi \le (2\pi r/r_0 + 2\phi) < 2\pi$, where r and ϕ are the polar radius and the azimuth angle in the plane of the wedged cell, respectively, and r_0 is the maximum radius of the designed pattern. This kind of vector polarizer was realized when the phase delay of the SLM is set to be $\delta = \pi - 2\phi$ during exposure. Using the experimental setup [Fig. 4(a)], we can characterize the fabricated vector polarizer [with the alignment pattern of the LC molecules as shown by the line segments in Fig. 5(a)] under the incidence of a circularly polarized wave. The captured intensity of the *e*-wave refracted from the vector polarizer [Fig. 5(a)] exhibits a nearly uniform top-hat profile. To analyze its spatial polarization states, the linearly polarized analyzers at 0°, 45°, and 90° are inserted in front of CCD, respectively. Clearly, behind the polarization analyzer, the simulated intensity patterns [Figs. 5(b)–5(d)] are in good agreement with the measured ones [Figs. 5(e)–5(g)]. When the analyzers are placed at 0° and 90°, the intensity patterns are composed of four uniformly distributed Archimedes spirals [Figs. 5(b), 5(d), 5(e), and 5(g)]. However, when the polarized analyzer is oriented at 45°, the intensity pattern is composed of two thin Archimedes spirals and four thick Archimedes spirals in pairs [Figs. 5(c) and 5(f)]. These results mean that the points with the same polarization in the cross section of the *e*-wave will form an Archimedes spiral,
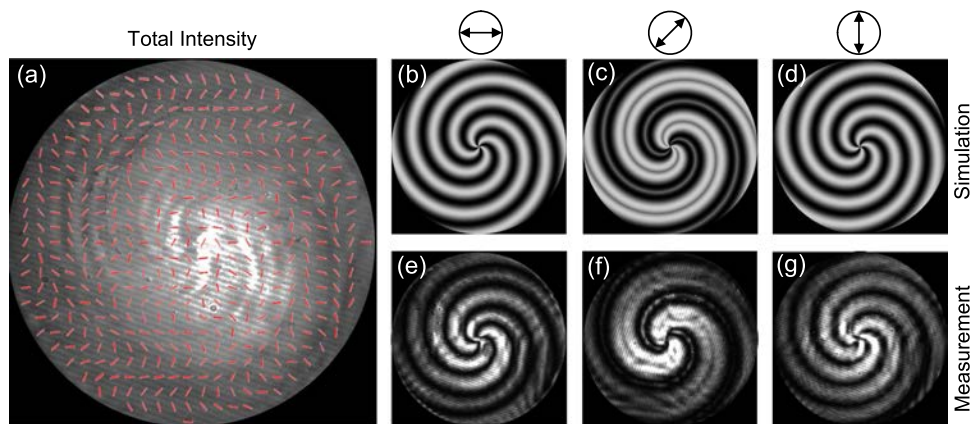

FIG. 5. Polarization modulation based on the Archimedes-spiral aligned vector polarizer under the incidence of circularly polarized wave. (a) Measured intensity pattern of the *e*-wave refracted from the Archimedes-spiral aligned vector polarizer, where the polarization pattern is shown by the line segments. [(b)–(d)] Simulated intensity patterns, when the linear polarizers at 0°, 45°, and 90° were inserted, respectively. [(e)–(g)] Measured intensity patterns corresponding to simulated results in (b)–(d), respectively. (a)–(g) have the same dimensions of 5×5 mm^2.

that is to say, the locations at an Archimedes spiral in the vector polarizer will also have the same alignment.

We also present the third demonstration, which is the "Pegasus" pattern composed of several parts [inset in Fig. 6(a)]. We designed and fabricated a vector polarizer with the "Pegasus" pattern. The alignment directions of LC molecules in different regions of the "Pegasus" pattern are oriented at 0°, 30°, 60°, 90°, 120°, 150°, and 180°, respectively [shown by arrows in Fig. 6(a)]. Using the experimental setup shown in [Fig. 4(a)], we test the designed and fabricated "Pegasus" vector polarizer under the incidence of the circularly polarized wave. The captured intensity of the *e*-wave from the vector polarizer [Fig. 6(a)] exhibits a nearly uniform distribution excluding some dividing lines, which originate from the different polarizations in two adjacent areas. To check the polarization pattern of the *e*-wave, the analyzers oriented at 0°, 45°, and 90° were inserted in front of CCD, respectively. For the above three cases, the intensity patterns become nonuniform, and the simulated intensity patterns [Figs. 6(b)–6(d)] are in good agreement with the intensity patterns measured by CCD [Figs. 6(e)–6(g)]. The results suggest that the polarization of the *e*-wave is parallel to the alignment direction of the vector polarizer, as shown by the arrows in Fig. 6(a).

C. Spatial modulation of intensity

Very interestingly and importantly, the vector polarizer we presented can also be used to realize arbitrarily spatial modulation in the intensity profile of the optical field. To verify this idea, as an example, we generated the zero-order Bessel beam[34] based on the vector polarizer. The key point is how to design and fabricate the desired vector polarizer. As mentioned above, if the incident light is linearly polarized in the *x* axis and the LC molecules filled in the vector polarizer are oriented at an angle φ with respect to the *x* axis, the intensity transmittance of the vector polarizer for the *e*-wave and *o*-wave (t_e and t_o) obeys the Malus' law as $t_e = \cos^2 \varphi$ and $t_o = \sin^2 \varphi$, respectively. As long as we have $t_e = J_0^2(\beta r) = \cos^2 \varphi$ for the fabricated vector polarizer, where r is the radial coordinate, β denotes a transverse component of a wave vector, and $J_0(\cdot)$ is the zero-order Bessel function of the first kind, hence the *e*-wave refracted from such a vector polarizer should be the zero-order Bessel beam. Of course, we can also generate the zero-order Bessel beam from the *o*-wave outputted from the vector polarizer when setting $t_o = J_0^2(\beta r) = \sin^2 \varphi$. The fabricated zero-order Bessel vector polarizer can be used to modulate the intensity of the incident beam at various wavelengths. Due to the dispersion effect of the LC material,[35] the deflection angle of the *e*-polarized zero-order Bessel beam will slightly change, so the position of the spatial filter needs to be slightly adjusted synchronously for picking up it. The measured intensity patterns of the *e*-polarized zero-order Bessel beam, outputted from the same zero-order Bessel vector polarizer under the incidence of linearly polarized wave, are shown
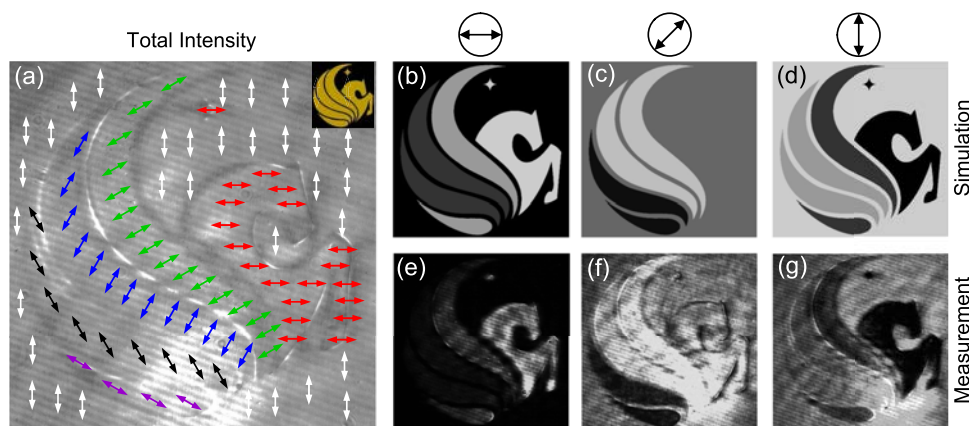

FIG. 6. Polarization modulation based on the "Pegasus" patterned vector polarizer under the incidence of the circularly polarized wave. (a) Measured intensity pattern of the *e*-wave refracted from the "Pegasus" patterned vector polarizer, where the polarization orientation at different regions are at 0°, 30°, 60°, 90°, 120°, 150°, and 180°, respectively. [(b)–(d)] Simulated intensity patterns when the linear polarizers at 0°, 45°, and 90° were inserted, respectively. [(e)–(g)] Measured intensity patterns corresponding to simulated results in (b)–(d), respectively. (a)–(g) have the same dimensions of 5 × 5 mm².
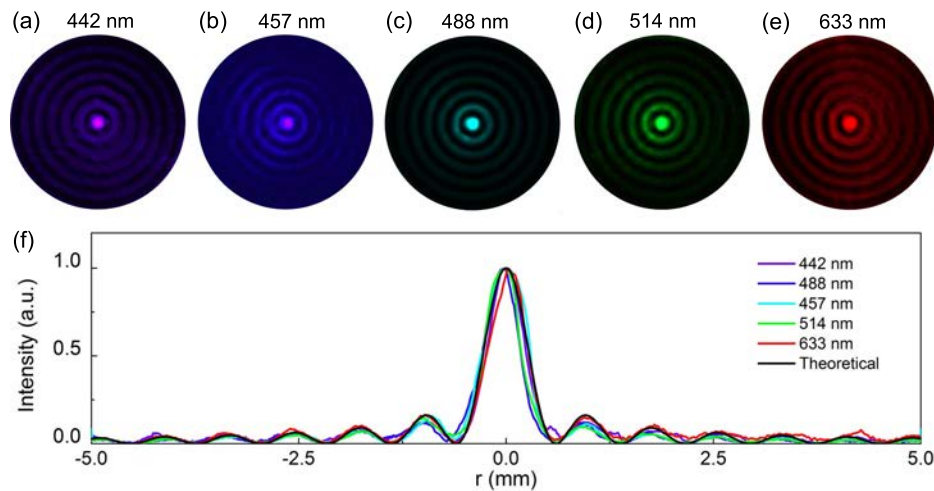
FIG. 7. Intensity modulation at multiple wavelengths based on the zero-order Bessel vector polarizer. The designed intensity profile is the zero-order Bessel beam, which is the output from the vector polarizer. (a)–(e) are the measured *e*-wave at λ = 442, 457, 488, 514, and 633 nm, respectively. (f) The intensity profiles corresponding to (a)–(e) in the radial direction.

in Fig. 7, at λ = 442, 457, 488, 514, and 633 nm, respectively. Clearly, the experimentally obtained zero-order Bessel beams are in good agreement with the theoretical prediction. It also implies that the fabricated vector polarizer can be used over a broadband wavelength and the intensity profiles for different wavelengths have almost no change [Fig. 7(f)].

IV. CONCLUSION

In conclusion, we theoretically designed and experimentally demonstrated the customized high-performance vector polarizer, which is realized by a LC-SV-UAC. The key for fabricating a LC-SV-UAC is to achieve the space-variant alignment of dye molecules in the dichroic dye films coated to the empty wedged cell, by using the polarization-sensitive photo-alignment technique. The LC molecules filled into the empty wedged cell will be aligned along the orientations of local dye molecules in the photo-aligned dye films. After the LC-filled empty wedged cell is sealed, the fabrication of the LC-SV-UAC is finally completed. Based on the birefringent effect and the prism effect of the wedge, the vector polarizer can spatially separate the orthogonally *o*- and *e*-polarized waves at different deflection angles, whose polarization directions are perpendicular and parallel to the space-variant alignment of LC molecules, respectively. The fabricated vector polarizer has the indirect flexibility, which is allowed to have the arbitrary space-aligned structure of the LC molecules because the VOF for photo-aligning the dichroic dye films can be deliberately designed and generated. Furthermore, the vector polarizer we presented can easily realize not only polarization structure but also the intensity modulation. In addition, the vector polarizer we proposed can be easily mass-produced and can work under different wavelengths. In particular, the LC-SV-UAC is used as not only a vector polarizer but also a generator of the VOF and a key element for realizing the VOF laser and for fabricating the novel photon states in the future, which has the high efficiency and the perfect polarization purity, because its working principle is based on the birefringent effect.

Finally, we give some discussions about the differences between the LC-SV-UAC and other liquid crystal based broadband modulator, such as the *q*-plate[36–38] and the space-variant twisted nematic LC cell.[39–41] For the *q*-plate,[36–38] its broadband property is normally realized through given different electric fields to tune its refractive index. In our device, no extra applied electric field is needed for various wavelengths. For the space-variant twisted nematic LC cell,[39–41] it also has the broadband property and no applied electric field is needed, like our device. However, it has the disclination lines in the obtained fields, which can be seen in the reported works,[40,41] so that it is not suitable for arbitrary modulation. Our wedged configuration design solved these problems.

ACKNOWLEDGMENTS

[1] D. Basu, *Dictionary of Pure and Applied Physics* (CRC Press, 2000).
[2] Q. Zhan, Adv. Opt. Photonics **1**, 1 (2009).
[3] H. Rubinsztein-Dunlop, A. Forbes, M. V. Berry, M. R. Dennis, D. L. Andrews, M. Mansuripur, C. Denz, C. Alpmann, P. Banzer, T. Bauer *et al.*, J. Opt. **19**, 013001 (2016).
[4] X. L. Wang, J. Chen, Y. Li, J. Ding, C. S. Guo, and H. T. Wang, Phys. Rev. Lett. **105**, 253602 (2010).
[5] Y. Pan, X. Z. Gao, Z. C. Ren, X. L. Wang, C. Tu, Y. Li, and H. T. Wang, Sci. Rep. **6**, 29212 (2016).
[6] D. B. Ruffner and D. G. Grier, Phys. Rev. Lett. **108**, 173602 (2012).
[7] K. Lou, S. X. Qian, Z. C. Ren, C. Tu, Y. Li, and H. T. Wang, Sci. Rep. **3**, 2281 (2013).
[8] M. Duocastella and C. B. Arnold, Laser Photonics Rev. **6**, 607 (2012).
[9] J. T. Barreiro, T. C. Wei, and P. G. Kwiat, Phys. Rev. Lett. **105**, 030407 (2010).
[10] X. L. Wang, X. D. Cai, Z. E. Su, M. C. Chen, D. Wu, L. Li, N. L. Liu, C. Y. Lu, and J. W. Pan, Nature **518**, 516 (2015).
[11] V. Kalosha and I. Golub, Opt. Lett. **32**, 3540 (2007).
[12] J. Fölling, M. Bossi, H. Bock, R. Medda, C. A. Wurm, B. Hein, S. Jakobs, C. Eggeling, and S. W. Hell, Nat. Methods **5**, 943 (2008).
[13] G. Milione, T. Wang, J. Han, and L. Bai, Chin. Opt. Lett. **15**, 030012 (2017).
[14] N. Cvijetic, G. Milione, E. Ip, and T. Wang, Sci. Rep. **5**, 15422 (2015).
[15] H. Huang, G. Milione, M. P. J. Lavery, T. A. Nguyen, D. A. Nolan, M. J. Li, M. J. Padgett, R. R. Alfano, and A. E. Willner, Sci. Rep. **5**, 14931 (2015).
[16] G. Milione, T. A. Nguyen, J. Leach, M. P. J. Lavery, E. Karimi, S. Slussarenko, L. Marrucci, M. J. Padgett, and R. R. Alfano, Opt. Lett. **40**, 4887 (2015).
[17] G. Milione, H. Huang, M. P. J. Lavery, T. A. Nguyen, D. A. Nolan, M. J. Li, E. Karimi, S. Slussarenko, L. Marrucci, R. R. Alfano, and A. E. Willner, Opt. Lett. **40**, 1980 (2015).
[18] X. L. Wang, J. Ding, W. J. Ni, C. S. Guo, and H. T. Wang, Opt. Lett. **32**, 3549 (2007).
[19] C. Maurer, A. Jesacher, S. Fürhapter, S. Bernet, and M. Ritsch-Marte, New J. Phys. **9**, 78 (2007).
[20] J. Liu and J. Wang, Sci. Rep. **5**, 9959 (2015).
[21] S. Liu, P. Li, T. Peng, and J. Zhao, Opt. Express **20**, 21715 (2012).
[22] W. Ji, C. H. Lee, P. Chen, W. Hu, Y. Ming, L. Zhang, T. H. Lin, V. Chigrinov, and Y. Q. Lu, Sci. Rep. **6**, 25528 (2016).
[23] L. Marrucci, C. Manzo, and D. Paparo, Phys. Rev. Lett. **96**, 163905 (2006).
[24] Z. Bomzon, G. Biener, V. Kleiner, and E. Hasman, Opt. Lett. **27**, 285 (2002).
[25] A. Arbabi, Y. Horie, M. Bagheri, and A. Faraon, Nat. Nanotechnol. **10**, 937 (2015).
[26] C. Pfeiffer and A. Grbic, Phys. Rev. Appl. **2**, 044012 (2014).
[27] M. Kang, J. Chen, X. L. Wang, and H. T. Wang, J. Opt. Soc. Am. B **29**, 572 (2012).
[28] R. Dorn, S. Quabis, and G. Leuchs, Phys. Rev. Lett. **91**, 233901 (2003).
[29] X. Hao, C. Kuang, T. Wang, and X. Liu, Opt. Lett. **35**, 3928 (2010).
[30] H. Wang, L. Shi, B. Lukyanchuk, C. Sheppard, and C. T. Chong, Nat. Photonics **2**, 501 (2008).
[31] Z. Bomzon, G. Biener, V. Kleiner, and E. Hasman, Opt. Lett. **26**, 1711–1713 (2001).
[32] M. Schadt, H. Seiberle, and A. Schuster, Nature **381**, 212 (1996).
[33] J. L. West, L. Su, and Y. Reznikov, Mol. Cryst. Liq. Cryst. Sci. Technol., Sect. A **364**, 199 (2001).
[34] D. McGloin and K. Dholakia, Contemp. Phys. **46**, 15 (2005).
[35] S. T. Wu, Phys. Rev. A **33**, 1270 (1986).
[36] Y. S. Rumala, G. Milione, T. Nguyen, S. Pratavieira, Z. Hossain, D. Nolan, S. Slussarenko, E. Karimi, L. Marrucci, and R. R. Alfano, Opt. Lett. **38**, 5083 (2013).
[37] F. Cardano, E. Karimi, S. Slussarenko, L. Marrucci, C. de Lisio, and E. Santamato, Appl. Opt. **51**, C1–C6 (2012).
[38] M. N. Miskiewicz and M. J. Escuti, Opt. Express **22**, 12691 (2014).
[39] M. Stalder and M. Schadt, Opt. Lett. **21**, 1948 (1996).
[40] P. Chen, W. Ji, B. Y. Wei, W. Hu, V. Chigrinov, and Y. Q. Lu, Appl. Phys. Lett. **107**, 241102 (2015).
[41] M. V. Vasnetsov, V. A. Pasko, and D. S. Kasyanyuk, Opt. Lett. **36**, 2134 (2011).